Hindawi
Mathematical Problems in Engineering
Volume 2019, Article ID 6240320, 8 pages
https://doi.org/10.1155/2019/6240320

Research Article

Computational Fluid Dynamics (CFD) Investigation of Aerodynamic Characters inside Nasal Cavity towards Surgical Treatments for Secondary Atrophic Rhinitis

Ya Zhang,[1] Xudong Zhou,[2] Miao Lou,[1] Minjie Gong,[1] Jingbin Zhang,[3] Ruiping Ma,[1] Luyao Zhang,[1] Fen Huang,[2] Bin Sun,[1] Kang Zhu,[1] Zhenbo Tong,[2] and Guoxi Zheng[1]

[1]*Department of Otolaryngology Head and Neck Surgery, The Second Affiliated Hospital of Xi'an Jiaotong University, Xi'an, Shaanxi, 710004, China*
[2]*School of Energy and Environment, Southeast University, Nanjing, Jiangsu, 210096, China*
[3]*Department of Imaging, The Second Affiliated Hospital of Xi'an Jiaotong University, Xi'an, China*

Correspondence should be addressed to Guoxi Zheng; zhengguoxi888@sina.com

Received 9 August 2019; Accepted 27 November 2019; Published 30 December 2019

Academic Editor: Hao Zhang

Purpose. To use computational fluid dynamics (CFD) technology to fundamentally understand (1) the effect of surgical treatments on nasal physiology for secondary atrophic rhinitis and (2) the priority of operations. *Subjects and Methods*: With the aid of medical imaging and CFD modeling, three virtual operations (nasoseptal perforation repair, cavity narrowing, and a combination of both) were performed to analyze airflow, nasal resistance, and wall shear stress. *Results*. Compared with the cavity-narrowing virtual operation, nasal resistance was not significantly altered by septal perforation repair virtual operation. Airflow allocation changed with more air flowing through the olfactory area and less though the nasal floor after all operations, especially the cavity-narrowing operation. Wall shear stress at the original epistaxis area and the nasal floor was reduced after the cavity-narrowing operation. *Conclusions*. Simulation results suggest that the cavity-narrowing operation takes priority over septal perforation repair if a staged surgery approach is adopted. If only one operation can be chosen, the cavity-narrowing operation is better than the septal perforation repair. This work shows that CFD-based modeling may aid precision medicine.

1. Introduction

Disorders of the nasal cavity are closely linked to its structure and function. Correction of morphological abnormalities of the nasal cavity is fundamental to the treatment of diseases. Secondary atrophic rhinitis (AR) is commonly caused by destructive nasal surgery [1, 2] and is characterized by progressive mucosal atrophy, nasal crusting, dryness, and enlarged nasal space with a paradoxical sensation of nasal congestion [2]. The disease is often accompanied by septal perforation, epistaxis, anosmia, depression, and sinusitis [2] and may seriously impair the patients' quality of life [3]. The disease is encountered by rhinologists all over the world and is particularly common in China [1, 2].

Medical treatments provide only symptomatic relief. With the developments in tissue engineering, surgical reconstruction of the nasal structure is a promising treatment to effect radical cure. But, simultaneous implantation of materials or tissues may cause problems like infection and nonhealing. Staging surgery is often used to prevent these problems. For patients with secondary atrophic rhinitis with nasal septum perforation, the cavity-narrowing operation and nasoseptal perforation repair operation are two common choices [4]. However, the optimal sequence for these operations is not clear.

With the development of the biological simulation methods, computational fluid dynamics (CFD) is increasingly gaining popularity as a powerful tool for performing virtual surgeries to test various scenarios and for selecting the proper procedure to achieve the optimal outcome. Rhinologists use this approach to simulate surgeries for deviation of the nasal septum, turbinectomy [3, 5, 6],

maxillary sinus ventilation [7], and nasal septum perforation repair [8]. Results indicate that it is a promising research method compatible with precision medicine [7, 8].

In this study, three operation plans have been simulated using CFD models (Virtual surgery 1: nasoseptal perforation repair operation, Virtual surgery 2: cavity-narrowing operation, Virtual surgery 3 = 1 + 2: both nasoseptal perforation repair and cavity narrowing). By analyzing the aerodynamic changes after different operations and comparing them with those in height- and weight-matched healthy volunteers, the effects of the three operations have been evaluated by the optimal sequence of operations. In addition, we implemented the surgical closure of the nasal septum perforation in a patient, based on CFD modeling. We summarize this clinical experience in this paper.

2. Materials and Methods

2.1. Patient and Healthy Control. The subject in our study was a 62-year-old Chinese woman who was a known case of atrophic rhinitis. The patient required repeated hemostatic laser treatment at the local hospital for frequent epistaxis, but without any symptom relief. The patient complained of nasal dryness and hyposmia with no purulent nasal discharge, nasal obstruction, nasal itching, sneezing, and whistling. Figure 1 shows the CT view, the endoscopic view, and the 3D modeling view of the nasal cavity. The septal perforation, the atrophied inferior turbinate, and the epistaxis area can be seen clearly. The coronal nasal computed tomography (CT) scan showed absence of inferior turbinate on both sides and a nasal septal perforation in anteroinferior part (defect size, $1.7 * 1.1$ cm, 1.6–3.3 cm from the nostril). Fiber-optic nasal endoscopy verified the diagnosis of nasal septum perforation and atrophied inferior turbinate. The T&T olfactometer was used to evaluate the sense of smell of the patient; the score was 2.8 points.

There was no history of allergic rhinitis, chronic heart and lung disease, or nasal trauma. The patient requested a nasoseptal perforation repair operation. After an effective control of nasal dryness, an autograft comprising three layers of temporal fascia, tragus cartilage, and artificial dura was fixed into the nasal septum using the "sandwich" technique (Figure 1(e)). One month after surgery, the patient reported an improved nasal ventilation and smell sensation. The T&T standard olfactometer score at this stage was 1.6 points. Repeat nasal coronal CT scan showed a partial closure of the nasal septal perforation (Figure 1(d)). There was a minor defect in the septum ($0.3 * 0.3$ cm; 3.2–3.5 cm from the nostril) and a shift of the perforation patch towards the right side. Comment: T&T olfactometer (score 1.1–2.5: mild loss of smell sensation, 2.6–4.0: medium loss, 4.1–5.4: heavy loss, and 5.5: complete loss of the smell sensation).

A height- and weight-matched healthy volunteer served as the control. We measured her nasal resistance using a six-phase rhinomanometer (GM) in inspiration and expiration. The result was 0.131 Pa * s/mL in inspiration. All subjects provided written informed consent for participation in this study. The study was approved by the institutional review board and the medical ethics committee at the second affiliated hospital of the Xi'an Jiaotong University.

2.2. Modeling and Simulation Conditions. Figure 2 depicts the perations and characteristics of models A, B, C, D, and E. Models A and E were based on pre- and postoperative high resolution computed tomography (CT) images of a female patient with secondary AR who was treated with nasoseptal perforation repair. Models B, C, and D were performed to mimic the virtual surgery 1, 2, and 3. Model F was based on a healthy female and served as the control. Red circles indicate preoperative positions of nasal septal perforation. Green circles indicate the positions of nasal septal perforation and postoperation. Black arrows indicate the positions of the cavity-narrowing operation.

Here, the 3D geometry of human nasal airways was reconstructed in four steps [9–13]. In the first step, CT-scan images were taken. In the second step, CT-scan images with DICOM format were processed by Mimics software and the boundary coordinates of the nasal cavities walls were identified. In the third step, the outcome of the image processing was imported into Geomagic software and the nasal airway volume was created. The 3D volume from Geomagic was then exported to the mesh generation software ICEM CFD (ANSYS, Inc.) to produce the 3D computational domain (Figure 3).

Mesh sensitivity tests were conducted to ensure grid independence for all results; data reported here were obtained in meshes of 600,000–1,200,000 tetra cells. The air flow is modelled by using the steady, laminar, incompressible, and isothermal Navier–Stokes equations. The second-order upwind scheme was used for spatial discretization.

Pressure-velocity coupling was resolved using the SIMPLE method. For all calculations, the airflows were assumed to be incompressible and steady. The inlet plane was below the nasopharynx and the outlet plane close to the nostril. A uniform velocity normal to the inlet plane was specified by the quiescent cyclic respiratory airflow rate of 250 mL/s [14] through the nasal cavity. The inlet velocity was of negative value during inspiration and positive during expiration. The gauge pressure at the outlet was maintained at one atmosphere pressure. The Reynolds number based on the inlet velocity and the nasopharynx diameter was approximately 1300, indicating that the flow was predominantly laminar. To make it reasonably simple, the laminar model was used in the simulation.

3. Results

The objectives of surgery are to reduce nasal cavity volume so as to increase nasal resistance, to reduce mucosal wall shear stress so as to decrease epistaxis, and to deviate airflow from the surgical site toward a healthy or nonoperated area [15].

3.1. Nasal Resistance. Nasal resistance (R_{nose}) was defined as $R_{\text{nose}} = \Delta p/Q$, where Δp is the pressure drop in pascals (Pa)

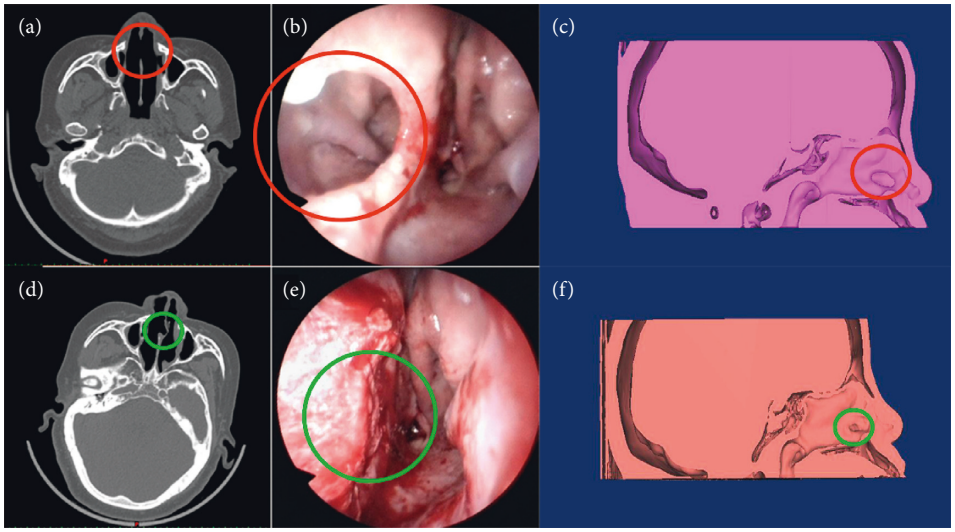

Figure 1: (a) Preoperative horizontal slice of CT data; (b) preoperative nasal endoscopy; (c) preoperative visualization of the respiratory airways in a midsagittal cut; (d) postoperative nasal CT scan after 1 month; (e) intraoperative nasal endoscopy; and (f) postoperative visualization of the respiratory airways in a midsagittal cut. Red circles indicate preoperative positions of nasal septal perforation. Green circles indicate the positions of nasal septal perforation, the postoperation.

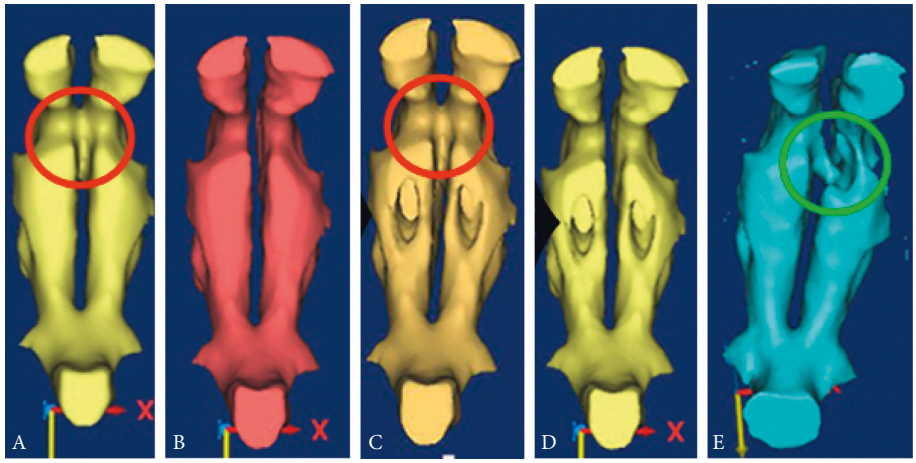

	Preop	Virtual surgery1	Virtual surgery2	Virtual surgery3	Postop
Model	Model A	Model B	Model C	Model D	Model E
Operation	None	Nasoseptal perforation rapair operation	Cavity-narrowing operation	Virtual surgery1 + 2	Nasoseptal perforation rapair operation

Figure 2: Operations and characteristics of models A, B, C, D, and E. Red circles indicate preoperative positions of nasal septal perforation. Green circles indicate the positions of nasal septal perforation, the postoperation. Black arrows indicate the positions of the cavity-narrowing operation.

and Q is the flow rate in milliliters per second (mL/s), which was computed from the simulation results and compared with data obtained on rhinomanometry [16, 17]. For the Model F, the CFD-calculated result closely matched the rhinomanometry-obtained result (0.117 Pa $*$ s/mL vs. 0.131 Pa $*$ s/mL). All the CFD-calculated total nasal resistance values are depicted in Table 1: Model F > Model C > Model D > Model E > Model B > Model A. So, in increasing the nasal resistance, Virtual surgery 2≈Virtual surgery 3 > Virtual surgery 1.

3.2. Airflow Streamlines

3.2.1. Olfactory Area. Airflow allocation indicates the percentage of total air passing through the olfactory area. As is shown in Table 1 and Figure 4, Model F > Model C > Model D > Model B > Model E > Model A.

It implied that Virtual surgery 2 > Virtual surgery 3 > Virtual surgery 1 > Postoperation > Preoperation.

Vortex: Model F > Model C > Model D > Model B > Model E > Model A. (Figure 4)

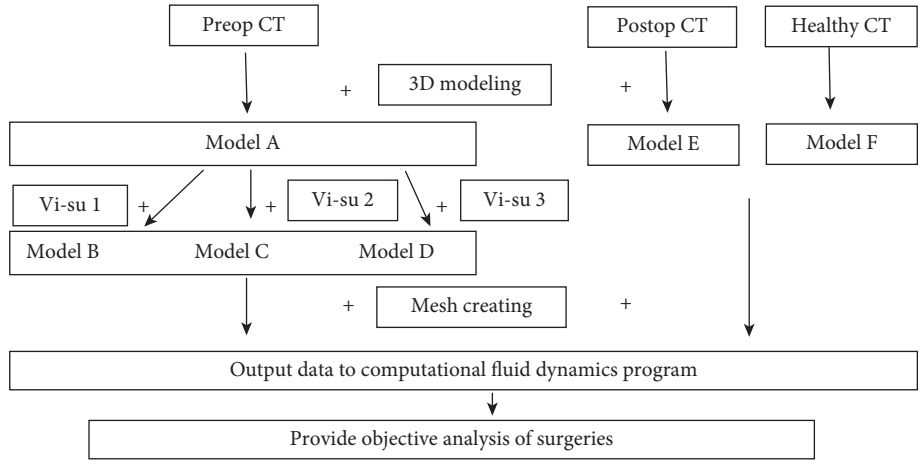

Figure 3: Technical route of the research.

Table 1: CFD-calculated total nasal resistance, resistance ratio, and airflow allocation.

	Model A	Model B	Model C	Model D	Model E	Model F
Total nasal resistance (Pa ∗ s/mL)	0.050	0.066	0.082	0.080	0.076	0.117
Nasal resistance ratio (%)	43.2%	56.8%	70.2%	68.8%	65.1%	100%
Airflow allocation (olfactory area)	13.1%	19.1%	21.5%	19.4%	14.2%	22.6%

It implied that Virtual surgery 2 > Virtual surgery 3 > Virtual surgery 1 > Postoperation > Preoperation.

3.2.2. Nasal Floor (Figure 4). There are large vortexes before operation (Model A). Thick nasal crusts appeared at this site. There are still large vortexes after virtual and real closure of perforation operation (Model B and Model E). However, there are few vortexes in healthy control and after virtual surgery 2 and 3 (models F, C, and D).

3.3. Mucosal Wall Shear Stress Contours (Pa). Wall shear stress is the tangential drag force produced by air moving across the mucosal surface. It is a function of the velocity gradient of air near the mucosal surface. The higher the wall shear force is, the greater damage the mucosa may suffer.

As is shown in Figure 5 and Table 2,

(1) Preoperation: the mucosal shear stress on the posterior inferior edge of the septal perforation is relatively higher than that at other edges of the septal perforation, which is consistent with the site of epistaxis and erosion (Figures 1 and 5)

(2) Virtual surgery 1 reduced the maximum mucosal wall shear stress at the nasal floor by 85% (0.253 Pa to 0.037 Pa)

(3) Virtual surgery 2 reduced the maximum mucosal wall shear stress in the original epistaxis area by 82% (0.330 Pa to 0.059 Pa) and reduced the maximum mucosal wall shear stress at the nasal floor by 77% (0.253 Pa to 0.059 Pa)

(4) In all models, the highest mucosal wall shear stress areas appeared on the nasal valve and the nasopharynx.

4. Discussion

In our study, both pre- and postoperations' nasal aerodynamics were obtained by CFD simulation. The changes in the models are generally consistent with the results from previous studies [18–20], e.g., nasal resistance, wall shear stresses, and streamlines. Filling the knowledge gap by obtaining the aerodynamic features associated with secondary AR after staged surgeries is one of the major contributions of our study.

As speculated by other researchers [21, 22], the occurrence of AR can be explained or at least partially attributable to the aerodynamic changes in the AR models. In the following part, we mainly focus on the aerodynamic origins of the development of AR and changes after different surgeries based on our findings.

4.1. Nasal Resistance. In this study, the preoperative nasal resistance was found to be 43.2% of the healthy nasal resistance, which increased to 56.8%, 70.2%, and 68.8% after nasoseptal perforation repair, cavity-narrowing operation, and that after both operations, respectively. In an earlier study, nasal resistance reportedly decreased to 64% of the healthy nasal resistance after resection of the inferior turbinate [23]. With respect to postsurgical nasal airway resistance, the effect of nasoseptal perforation repair on increasing resistance is much less than that of cavity-narrowing surgery.

Therefore, cavity-narrowing surgery is better than nasoseptal perforation repair for increasing nasal resistance.

4.2. The Olfaction. In our case, the preoperative airflow reaching the olfactory area was very limited. In addition,

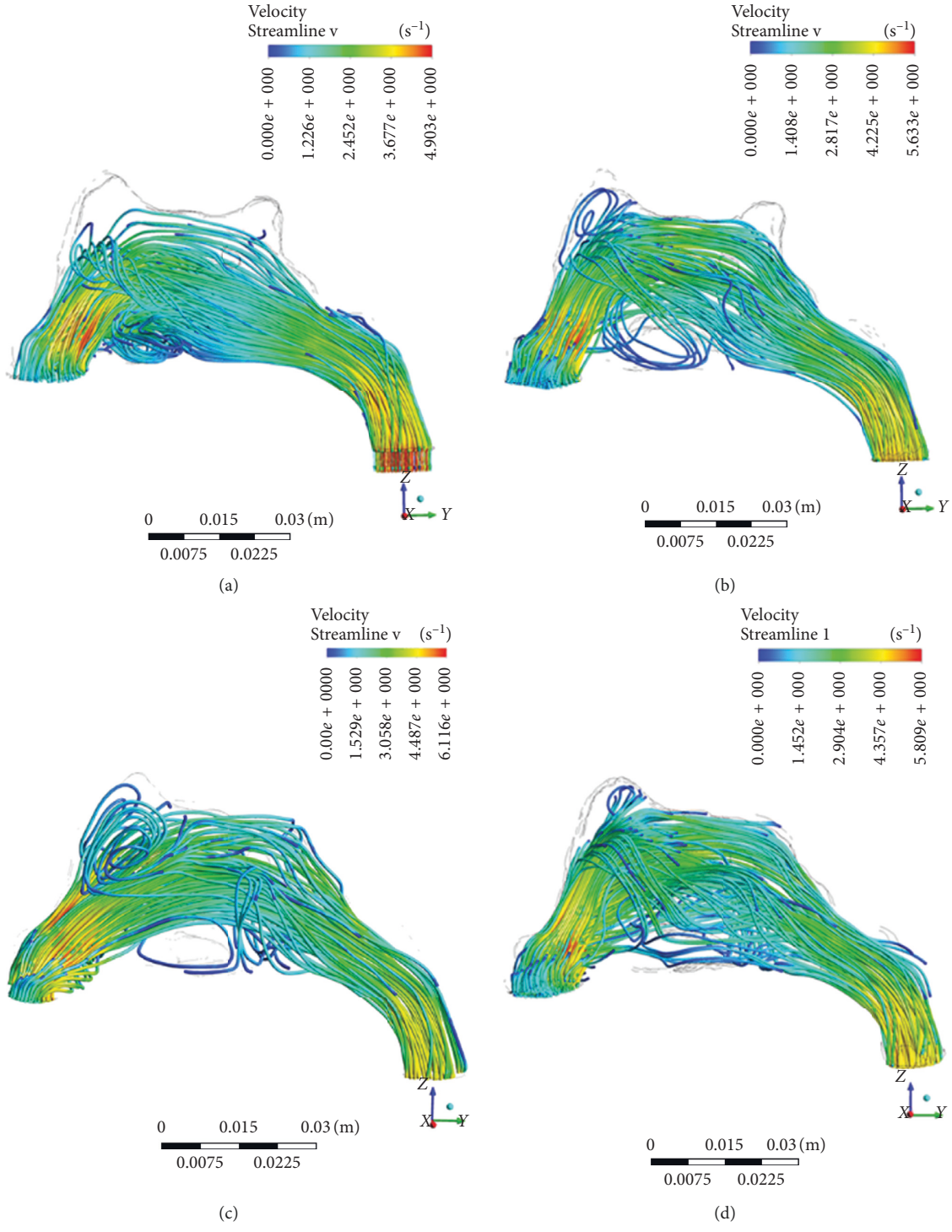

Figure 4: Continued.

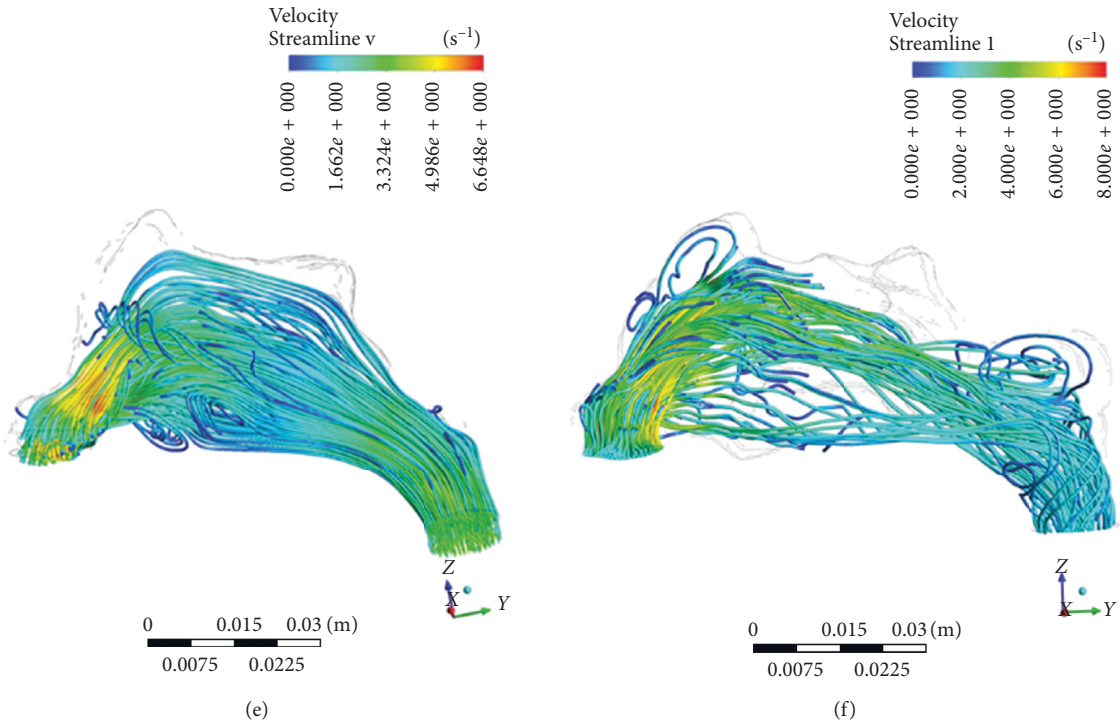

Figure 4: Comparison of airflow density path lines.

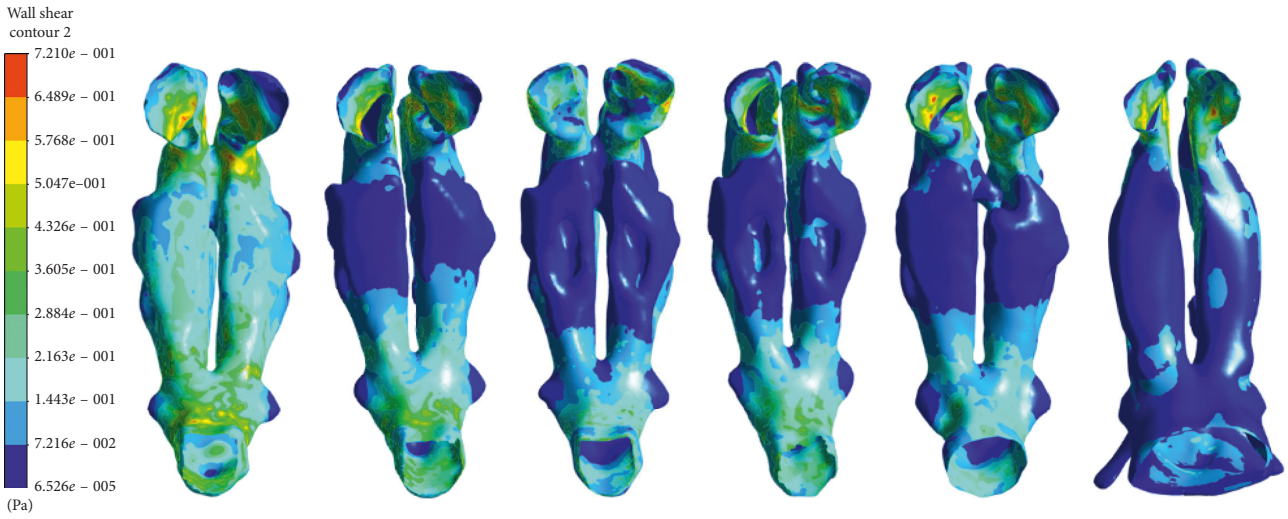

Figure 5: Comparison of mucosal wall shear stress contours (Pa).

Table 2: CFD-calculated wall shear stress.

Maximum wall shear stress (Pa)	Model A	Model B	Model C	Model D	Model E	Model F
Nasal floor	0.253	0.037	0.059	0.041	0.047	0.110
Septal perforation	0.330	—	0.059	—	0.095	—

pathological dryness in nasal cavity and dry crust formation in the olfactory area also impaired the smell sensation (preoperative score: 2.8 points, T&T olfactometer). Virtual surgery 1, 2, and 3 were associated with increased vortexes and airflow reaching the olfactory area, thus increasing the deposition of odorants in the olfactory area. This presumably resulted in an improved smell sensation (postoperative score, 1.6 points).

Stream flow in the olfactory area: Model C > Model B; therefore, cavity-narrowing surgery led to a greater increase

in nasal olfaction as compared with that observed after nasoseptal perforation repair.

4.3. Dryness and Nasal Crusting. In the Model A, more chaotic streamlines and new vortexes were observed near the bottom of the nasal cavity (Figure 3), a frequent site area of crusting in patients with atrophic rhinitis. More water vapors are redirected away by the chaotic airflow and vortexes [24–26]. Furthermore, the nasal mucosal area in our patient ($137.4\,cm^2$) was smaller than that in an average healthy Chinese woman ($160\,cm^2$), and the nasal mucosal size to volume ratio ($0.36\,mm^{-1}$) was much smaller than that in a healthy Chinese woman ($0.58 \pm 0.09\,mm^{-1}$) [27]. Therefore, the volume of air humidified per unit area of the nasal mucosa was reduced, thus resulting in increased dryness and crust formation [24].

After surgical closure of septal perforation, large vortexes were still observed. Cavity-narrowing surgery is more effective in eliminating vortexes. Therefore, the cavity-narrowing surgery is better than the nasoseptal perforation repair operation in decreasing nasal crusting.

4.4. Epistaxis. The anteroinferior part of the nasal septum, also referred to as Little's area, is susceptible to epistaxis [28, 29]. Studies based on CFD modeling have demonstrated a much higher shear stress over Little's area, thus contributing to its propensity for spontaneous epistaxis [30]. Cannon et al. [31] performed virtual surgery using a simulated septal perforation model. They documented highest shear force at the lateral edge of the perforation, which is consistent with our findings. Furthermore, the vortex increased the deposition of pathogens and physical and chemical particles, thereby increasing mucosal damage.

The cavity-narrowing surgery reduced the mucosal wall shear stress and vortexes at the edges of the septal perforation, so it can be concluded that the epistaxis can be eased after this surgery.

4.5. Perforation. Perforations in the septum do not typically heal on their own, and surgical treatment of nasal septal perforation remains a challenging field of rhinology. High mucosal wall shear stress at the open edge of the perforation may be a reason why it does not easily heal. Furthermore, after surgical closure of perforation, the mucosal wall shear stress over the site of perforation is still high, which impacts graft survival. However, cavity-narrowing surgery can reduce the mucosal wall shear stress and provide favorable conditions for graft survival, thus reducing the probability of reperforation.

5. Conclusion

Based on 6 different nasal structures, we examined the aerodynamic features in three typical nasal structures associated with secondary AR after different surgeries, which has not been studied and compared before. The observed changes in nasal aerodynamics can explain the underlying mechanisms involved in causing the typical symptoms in patients with secondary AR. Nasal aerodynamics appear to be instrumental in the pathogenesis of secondary AR. Thus, restoration of nasal aerodynamics should be a key consideration in the selection of the surgical approach.

Simultaneous cavity-narrowing operation and nasoseptal perforation repair operation can not only improve the flow field but also prevent the deterioration of the saddle nose. However, simultaneous implantation of materials or tissues may result in complications such as infection and nonhealing. Staged surgical approach may be beneficial wherein the cavity-narrowing operation should take precedence over the septal repair. If only one surgery is to be chosen, the cavity-narrowing operation is better. The exponential advancements in computing technology raise the hope that CFD analysis may be a viable and practical adjunct to nasal airway surgery in the near future.

Abbreviations

AR: Atraphic rhinitis
CFD: Computational fluid dynamics
CT: Computed tomography
3D: Three dimensional
Vi-su: Virtual surgery
Preop: Preoperation
Postop: Postoperation

Data Availability

The CT data used to support the findings of this study are restricted by the institutional review board and the medical ethics committee at the second affiliated hospital of the Xi'an Jiaotong University in order to protect patient privacy. Data are available from (Guoxi Zheng, zhengguoxi888@sina.com) for researchers who meet the criteria for access to confidential data.

Disclosure

No outside interest was paid for any part of this study.

Conflicts of Interest

The authors declare that they have no conflicts of interest.

Acknowledgments

This work was financially supported by the National Natural Science Foundation of China (no. 81271057) and Interdiscipline Subject of Xi'an Jiaotong University (no. 08143039).

References

[1] L. E. Jackson and J. R. Koch, "Controversies in the management of inferior turbinate hypertrophy: a comprehensive review," *Plastic and Reconstructive Surgery*, vol. 103, no. 1, pp. 300–312, 1999.

[2] E. J. Moore and E. B. Kern, "Atrophic rhinitis: a review of 242 cases," *American Journal of Rhinology*, vol. 15, no. 6, pp. 355–361, 2001.

[3] X. B. Chen, H. P. Lee, V. F. H. Chong, and D. Y. Wang, "Aerodynamic characteristics inside the rhino-sinonasal cavity after functional endoscopic sinus surgery," *American Journal of Rhinology & Allergy*, vol. 25, no. 6, pp. 388–392, 2011.

[4] M. T. Friji, S. Gopalakrishnan, S. K. Verma, P. K. Parida, and D. P. Mohapatra, "New regenerative approach to atrophic rhinitis using autologous lipoaspirate transfer and platelet-rich plasma in five patients: our Experience," *Clinical Otolaryngology*, vol. 39, no. 5, pp. 289–292, 2014.

[5] S. Zachow, A. Steinmann, T. Hildebrandt, R. Weber, and W. Heppt, "CFD simulation of nasal airflow: towards treatment planning for functional rhinosurgery," *International Journal of Computer Assisted Radiology and Surgery*, vol. 1, pp. 165–167, 2006.

[6] J. S. Kimbell, D. O. Frank, P. Laud, G. J. M. Garcia, and J. S. Rhee, "Changes in nasal airflow and heat transfer correlate with symptom improvement after surgery for nasal obstruction," *Journal of Biomechanics*, vol. 46, no. 15, pp. 2634–2643, 2013.

[7] K. J. Choi, D. W. Jang, M. D. Ellison, and D. O. Frank-Ito, "Characterizing airflow profile in the postoperative maxillary sinus by using computational fluid dynamics modeling: a pilot study," *American Journal of Rhinology & Allergy*, vol. 30, no. 1, pp. 29–36, 2016.

[8] T. Nomura, M. Ushio, K. Kondo, and T. Yamasoba, "Effects of nasal septum perforation repair surgery on three-dimensional airflow: an evaluation using computational fluid dynamics," *European Archives of Oto-Rhino-Laryngology*, vol. 272, no. 11, pp. 3327–3333, 2015.

[9] F. Huang, Y. Zhang, Z. B. Tong, X. L. Chen, R. Y. Yang, and A. B. Yu, "Numerical investigation of deposition mechanism in three mouth–throat models," *Powder Technology*, 2018.

[10] H. Zhang, B. Xiong, A. Xizhong, K. Chunhai, and J. Chen, "Numerical prediction on the drag force and heat transfer of non-spherical particles in supercritical water," *Powder Technology*, 2019.

[11] H. Zhang, B. Xiong, X. An, C. Ke, and G. Wei, "Numerical investigation on the effect of the incident angle on momentum and heat transfer of spheroids in supercritical water," *Computers & Fluids*, vol. 179, pp. 533–542, 2019.

[12] Y. Zhang, Y. Shang, K. Inthavong et al., "Computational investigation of dust mite allergens in a realistic human nasal cavity," *Inhalation Toxicology*, vol. 31, no. 6, pp. 224–235, 2019.

[13] Y. Zhang, "Computational investigation of Artemisia pollen deposition in realistic nasal cavities of residents in northwest China," *Zhonghua Er Bi Yan Hou Tou Jing Wai Ke Za Zhi*, vol. 54, no. 10, pp. 741–747, 2019.

[14] Y. Na, K. S. Chung, S. K. Chung, and S. K. Kim, "Effects of single-sided inferior turbinectomy on nasal function and airflow characteristics," *Respiratory Physiology & Neurobiology*, vol. 180, no. 2-3, pp. 289–297, 2012.

[15] S. M. Houser, "Empty nose syndrome associated with middle turbinate resection," *Otolaryngology-Head and Neck Surgery*, vol. 135, no. 6, pp. 972-973, 2006.

[16] J. S. Kimbell, G. J. M. Garcia, D. O. Frank, D. E. Cannon, S. S. Pawar, and J. S. Rhee, "Computed nasal resistance compared with patient-reported symptoms in surgically treated nasal airway passages: a preliminary report," *American Journal of Rhinology & Allergy*, vol. 26, no. 3, pp. e94–e98, 2012.

[17] B. Louis, J.-F. Papon, C. Croce et al., "Frictional resistance sheds light on the multicomponent nature of nasal obstruction: a combined in vivo and computational fluid dynamics study," *Respiratory Physiology & Neurobiology*, vol. 188, no. 2, pp. 133–142, 2013.

[18] S. C. Leong, "The clinical efficacy of surgical interventions for empty nose syndrome: a systematic review," *The Laryngoscope*, vol. 125, no. 7, pp. 1557–1562, 2015.

[19] N. Velasquez, Z. Huang, I. M. Humphreys, and J. V. Nayak, "Inferior turbinate reconstruction using porcine small intestine submucosal xenograft demonstrates improved quality of life outcomes in patients with empty nose syndrome," *International Forum of Allergy & Rhinology*, vol. 5, no. 11, pp. 1077–1081, 2015.

[20] T.-J. Lee, C.-H. Fu, C.-L. Wu et al., "Evaluation of depression and anxiety in empty nose syndrome after surgical treatment," *The Laryngoscope*, vol. 126, no. 6, pp. 1284–1289, 2016.

[21] G. J. M. Garcia, N. Bailie, D. A. Martins, and J. S. Kimbell, "Atrophic rhinitis: a CFD study of air conditioning in the nasal cavity," *Journal of Applied Physiology*, vol. 103, no. 3, pp. 1082–1092, 2007.

[22] Z. Zheng, H. Liu, Q. Xu et al., "Computational fluid dynamics simulation of the upper airway response to large incisor retraction in adult class I bimaxillary protrusion patients," *Scientific Reports*, vol. 7, Article ID 45706, 2017.

[23] X. B. Chen, "Aerodynamic effects of inferior turbinate surgery on nasal airflow—a computational fluid dynamics model," *Rhinology*, vol. 48, no. 4, pp. 394–400, 2010.

[24] D. Elad, M. Wolf, and T. Keck, "Air-conditioning in the human nasal cavity," *Respiratory Physiology & Neurobiology*, vol. 163, no. 1–3, pp. 121–127, 2008.

[25] M. O. Scheithauer, "Surgery of the turbinates and "empty nose" syndrome," *GMS current topics in otorhinolaryngology, head and neck surgery*, vol. 9, 2010.

[26] M.-Y. Di, Z. Jiang, Z.-Q. Gao, Z. Li, Y.-R. An, and W. Lv, "Numerical simulation of airflow fields in two typical nasal structures of empty nose syndrome: a computational fluid dynamics study," *PLoS One*, vol. 8, no. 12, Article ID e84243, 2013.

[27] H. Zang, Y. X. Liu, L. Zhang et al., "Nasal cavity computer fluid dynamics analysis on 60 healthy Chinese adults," *Zhonghua Er Bi Yan Hou Tou Jing Wai Ke Za Zhi*, vol. 48, no. 10, pp. 814–817, 2013.

[28] M. Supriya, M. Shakeel, D. Veitch, and K. W. Ah-See, "Epistaxis: prospective evaluation of bleeding site and its impact on patient outcome," *The Journal of Laryngology & Otology*, vol. 124, no. 7, pp. 744–749, 2010.

[29] S. K. Nitek, J. Wysocki, and C. S. Niszczota, "Use of transseptal mattress suture of Little's area for anterior epistaxis," *The Journal of Laryngology & Otology*, vol. 125, no. 4, pp. 399–401, 2011.

[30] N. Bailie, B. Hanna, J. Watterson, and G. Gallagher, "A model of airflow in the nasal cavities: implications for nasal air conditioning and epistaxis," *American Journal of Rhinology & Allergy*, vol. 23, no. 3, pp. 244–249, 2009.

[31] D. E. Cannon, D. O. Frank, J. S. Kimbell, D. M. Poetker, and J. S. Rhee, "Modeling nasal physiology changes due to septal perforations," *Otolaryngology-Head and Neck Surgery*, vol. 148, no. 3, pp. 513–518, 2013.